Muon contact hyperfine field in metals: A DFT calculation

Ifeanyi John Onuorah,[1] Pietro Bonfà,[2] and Roberto De Renzi[1,*]
[1]*Department of Mathematical, Physical and Computer Sciences, University of Parma, Parco Area delle Scienze 7/A, 43124 Parma, Italy*
[2]*CINECA, Casalecchio di Reno 6/3, 40033 Bologna, Italy*

(Received 30 March 2018; revised manuscript received 27 April 2018; published 15 May 2018)

In positive muon spin rotation and relaxation spectroscopy it is becoming customary to take advantage of density functional theory (DFT) based computational methods to aid the experimental data analysis. DFT-aided muon site determination is especially useful for measurements performed in magnetic materials, where large contact hyperfine interactions may arise. Here we present a systematic analysis of the accuracy of the *ab initio* estimation of muon's hyperfine contact field on elemental transition metals, performing state-of-the-art spin-polarized plane-wave DFT and using the projector-augmented pseudopotential approach, which allows one to include the core state effects due to the spin ordering. We further validate this method in not-so-simple, noncentrosymmetric metallic compounds, presently of topical interest for their spiral magnetic structure giving rise to skyrmion phases, such as MnSi and MnGe. The calculated hyperfine fields agree with experimental values in all cases, provided the spontaneous spin magnetization of the metal is well reproduced within the approach. To overcome the known limits of the conventional mean-field approximation of DFT on itinerant magnets, we adopt the so-called reduced Stoner theory [L. Ortenzi *et al.*, Phys. Rev. B **86**, 064437 (2012)]. We establish the accuracy of the estimated muon contact field in metallic compounds with DFT and our results show improved agreement with experiments compared to those of earlier publications.

DOI: 10.1103/PhysRevB.97.174414

I. INTRODUCTION

Muon spin rotation spectroscopy (μSR) is widely employed to investigate new strongly correlated electron materials, whose spin and orbital correlations display interesting temperature behavior that may show up directly in the experimental muon decay anisotropy. A significant advancement in modeling of μSR data stems from the knowledge of the muon site, not granted *a priori* and often provided by density functional theory (DFT) calculations since the advent of high-performance computing (HPC). It allowed, just to quote a few notable examples, the precise identification of specific muon bonds in insulators [1,2], the identification of deep and shallow hydrogen states in semiconductors [3,4], the pressure-induced magnetic structure in MnP [5], and the determination of infrequent subtle muon-induced effects in rare-earth pyrochlores [6].

However, the crucial point that provides *quantitative* access to electronic spin degrees of freedom is the full knowledge of the muon couplings with its surroundings. The often missing key ingredient is the contact hyperfine interaction, notably relevant in metals. This quantity may be calculated by *ab initio* techniques, but in practice the few published results date back to the early developments of DFT.

Only the determination of the muon implantation site *and* of the interaction constants between the muon and its atomic surrounding give access to crucial material properties such as the value of the ground-state ion magnetic moment in ordered materials and possibly the magnetic structure as well. Although μSR cannot compete with diffraction techniques for magnetic structure determination, there are cases where the latter are not applicable (due to the presence of either strong incoherent scatterers or neutron absorbers) [7] or not sufficient for a complete determination [5]. A noteworthy example is provided by the recent refinement of an additional structural parameter in the zero-field cycloid state of MnSi and its skyrmion phase, a nonvanishing phase between the two Mn orbits in the cycloid [8,9], inaccessible to neutrons, whose determination by μSR is made possible by the low symmetry of the muon site. The knowledge of both site and contact couplings is essential for this information to be retrieved.

Here we provide a demonstration of the effectiveness of a DFT-based approach, validated by the comparison with available experimental determinations. Five materials are selected by this criterion from the literature, ranging from simple magnetic metals, Fe, Co, Ni, to two additional chiral magnets of current high interest, MnSi and MnGe. The list of metals where the hyperfine coupling is experimentally known is unfortunately scarce, since they require quite accurate and time-consuming experiments on single crystals, and this is actually an additional motivation for validating a more general *ab initio* method.

The structure of the paper is the following: Section II briefly reviews the experimental technique highlighting the requirements for the theoretical approaches together with the most significant recent improvements. In Sec. II we analyze the different computational aspects that allow us to obtain converged results. In Sec. III we discuss our results, distinguishing the three elemental transition metals, Fe, Ni, and Co, used as a benchmark of the theoretical approximations from the case of the two additional metallic materials of current interest, MnSi and MnGe.

*roberto.derenzi@unipr.it

Finally, we discuss additional possible refinements to further reduce the difference between calculated and measured values.

II. μSR AND THE MUON COUPLINGS

μSR exploits the implantation of spin-polarized muons to probe local properties of materials by means of the local magnetic field at the muon, together with its dynamics on the scale of the muon's mean lifetime (∼2.2 μs). Notably, this experimental technique makes predominant use of the positive antiparticles (μ^+). The basis of this technique lies in the anisotropic positron emission at the muon decay, peaked around the muon spin direction. The anisotropy is a hallmark of weak interactions in the three-body decay, and the very high muon spin polarization (almost 100%) relies on the same violation in the two-body pion decay that originates this probe particle. The evolution of the muon spin direction may be thus detected over several microseconds, with very fine time resolution, over an ensemble of individually implanted particles. Thus, μSR may be considered akin to NMR, with the advantage of a broader applicability and a nonresonant broadband detection. The foremost applications are in superconducting and magnetic materials, including very weak magnets, thanks to the good sensitivity provided by the large muon gyromagnetic ratio (∼135 MHz/T) [10,11].

Implanted muons thermalize in inorganic crystalline solids almost invariably at interstitial sites in the lattice, so that the detected internal field is that at an interstitial, extremely diluted impurity. The experimental value of the muon local field, including both its static value and its fluctuating dynamical components, provides important clues towards understanding the magnetic properties of the host material. The muon local field both in superconductors and in magnetically ordered materials yields the temperature dependence of the order parameter, critical fluctuations are reflected in relaxation rates, and the presence of additional phase transitions is easily detected, just to quote a few examples. All these properties are directly accessed from the μSR spectra without any prior knowledge of the muon site and the details of its couplings.

In the following we shall refer explicitly to the investigation of magnetic materials, a specialty of μSR. Typically, here any refinement of the analysis does require additional *a priori* knowledge of the muon implantation site.

Ab initio DFT prediction of the muon site has been successfully employed in several studies, starting from the early pioneering investigations to the present, more extensive, although not yet everyday use, as detailed in a few reviews on the subject [1,12,13]. Site assignment is the key initial ingredient in the not infrequent cases where the internal magnetic field is dominated by the distant dipole contribution, which requires only the knowledge of the site in order to be computed by a classical sum over the dipole moments of the host lattice [10,11,14]. Thus, the comparison between predicted and measured local field can validate the muon site assignment, and in turn, this assessment yields, e.g., a measure of the magnetic moment values. However, additional local field contributions exist and they are not negligible in many cases. Thus, a nontrivial *ab initio* calculation of the couplings, besides its intrinsic value, in some cases is crucial for the site validation itself.

The contributions to the experimental local field, besides the already mentioned dominant dipolar sums, include another trivial term that is shape dependent (demagnetization) and proportional to the macroscopic sample magnetization [11]. We shall concentrate here on the contributions that require a quantum-mechanical description of the host electrons in the vicinity of the probe. In a localized spin magnet, they may give rise to direct transferred and super-transferred couplings, depending on whether the wave-function overlap between the muon probe and the magnetic ion is direct or through the polarization of the wave functions of intervening ligands. In metals, the conduction electrons provide an example of the first kind, giving rise to a contact interaction term that results in a spin density at the muon site. For the purpose of this paper we will focus only on the contact hyperfine interaction at the muon.

In the absence of external magnetic field and within a nonrelativistic quantum-mechanical description, the local field resulting from the interaction between the muon and an s electron at distance $r_{e-\mu} \to 0$ from the muon is described by the following Hamiltonian [15]:

$$\mathcal{H} = \frac{2\mu_0}{3}\gamma_e\gamma_\mu\hbar^2\mathbf{S}_\mu\mathbf{S}_e\delta(\mathbf{r}), \tag{1}$$

where μ_0 is the vacuum permeability, γ_e and γ_μ are the electron and muon gyromagnetic ratio, respectively, while $\mathbf{S}_e$ and $\mathbf{S}_\mu$ are their spin operators. It has been assumed that the muon is pointlike. In the collinear spin approximation, by integrating over the electron coordinates, the contact hyperfine field at the muon B_c is [16]

$$B_c = \tfrac{2}{3}\mu_0\mu_B\rho_s(\mathbf{r}_\mu), \tag{2}$$

where μ_B is the Bohr magneton, and the spin density ρ_s is defined as $(\rho_\uparrow(\mathbf{r}_\mu) - \rho_\downarrow(\mathbf{r}_\mu))$, with $\rho_\uparrow$ and $\rho_\downarrow$ being the density associated to each spinor component at the muon site $\mathbf{r}_\mu$. This equation was used to evaluate the contact field at the muon with the spin polarization obtained from DFT simulations.

The first principle theory of the hyperfine parameters for both heavy and light nuclei in magnetic materials is in principle well understood and has been studied since the mid 1960s [17–27]. Various approaches were proposed to improve the accuracy of the calculated contact fields, but these investigations, in particular for the muon in metals, were undertaken when computing resources were orders of magnitude less powerful than today. Their results are compared with our calculations in Sec. III. More recently valuable theoretical improvements [28–33] have established DFT as the standard for the calculation of NMR shift parameters, most reliably in nonmagnetic insulators. However, these improved methods were never directly applied to the muon case in metals. The main difference, as already noted, is that the location of the nuclei is extremely well known from diffraction, whereas the determination of the muon site is part of the same DFT problem, requiring in addition large supercells to represent the ideally diluted impurity while keeping an accurate description of the bulk sample. With the current availability of HPC it is well due to extend these modern methods to muon studies

in metallic systems in order to establish their accuracy and applicability.

Calculation details

The pseudopotential and plane-waves (PW) basis approach as in the QUANTUM ESPRESSO suite of codes were used for our calculations [40]. PW-based codes have a number of important features, namely, good parallel performances, good accuracy for the description of the bulk material, and simplicity of the basis set. The plane-wave basis is generally used to describe artificially smooth pseudo wave functions, thus avoiding the strong oscillations in the core region. Nonetheless, the projector augmented-wave (PAW) method introduced by Blóchl [3,27,41,42] allows one to approximate the all-electron density using a frozen-core reconstruction starting from the pseudo wave function. In the context of the PW basis, the PAW reconstruction method is therefore the method of choice for an accurate evaluation of Eq. (2). Since periodic boundary conditions are implied in the description of the bulk system, the effect of the extremely diluted muons in the material must be modeled within the supercell approximation, which reduces the artificial interactions between the charged impurities. It must be carefully verified that these artificial interactions of the muon periodic images are negligible on the quantities under study.

For all the calculations in this work, the plane-wave cutoffs were always above 100 Ry, granting a convergence on total energy (threshold 10^{-4} Ry) and spin density, while the exchange-correlation functionals were treated within the semilocal generalized gradient approximation (GGA) using the Perdew-Burke-Ernzerhof (PBE) formalism [43]. The calculations were done in the scalar relativistic approach, neglecting spin-orbit coupling. The scalar relativistic approximation is sufficient for the theoretical calculation of the muon contact field, since hydrogen (hence the muon) has a small nuclear charge and the contact field is predominantly due to on-site contributions of s-like states surrounding the muon [26,44,45]. The Marzari-Vanderbilt [46] smearing function was used.

A uniform Monkhorst-Pack [47] mesh was used for the k points. The convergence of the contact field depends strongly on the density of the mesh of k points. A $16 \times 16 \times 16$ mesh grid was used for the unit cell of the transition metals and a $12 \times 12 \times 12$ grid for the unit cell of the B20 compounds. The mesh sizes were selected following a systematic test to ensure independence of the size used to the spin density and total energies. These grids were downscaled proportionally for each supercell size.

The first step for all calculations involves the optimization of the structure and the correct reproduction of the electronic and magnetic properties of the pristine material. The next step involves investigating the extent of the lattice distortion around the muon and its influence on the electronic and magnetic properties of the nearest neighbors. The muon was introduced as hydrogen while maintaining a neutral cell considering that in metals, positive charges are effectively screened by the conduction electrons, enforcing charge neutrality of the whole system [1,2,12].

Before systematically comparing calculations with experimental values, let us further notice that we expect our results to overestimate the experimental absolute value, in view of the light mass of the muon, which results in relatively large amplitude of zero-point vibrations [48]. The muon behaves as a quantum oscillator, and the extent of its wave function is completely neglected in the *static* contact field from the DFT approach. The experimental value should be compared to the average over the muon wave function, whose accurate determination will be addressed separately and is beyond the scope of the present paper.

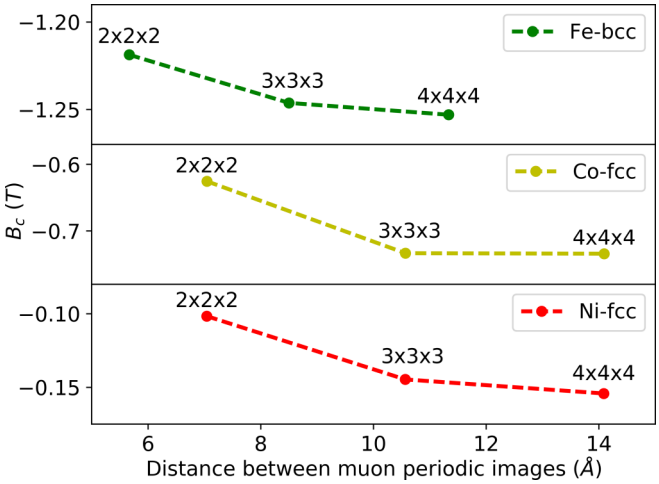

FIG. 1. Convergence of the muon contact hyperfine field B_c with the distance between muon periodic images for host systems of Fe, Ni, and Co. The x, y, z dimensions are the supercell sizes with reference to the unit cells.

III. RESULTS AND DISCUSSION

The appropriate size of the supercell for each of the materials was carefully determined considering convergence of the total DFT energies, distortion of the lattice and magnetic coupling in the vicinity of the muon, and in particular, the calculated contact hyperfine field, as shown in Fig. 1. The plot shows that this quantity converges at the $3 \times 3 \times 3$ cell level; however, we will compare results on the transition metals obtained with $4 \times 4 \times 4$ cells. Following the same systematic tests, a $2 \times 2 \times 2$ cell was used for the B20 compounds. Incidentally, in these metals convergence is achieved when the muon periodic replica are above 8.48 Å apart.

Next, we address the issue of whether the relaxation of the host atoms in the supercell including the muon has a significant effect on the quantity of interest. This is obtained comparing muon contact field values B_c with and without atomic relaxation. The results indicate that the relaxation around the muon significantly affects only the positions of the nearest-neighbor ions. The distortions are short ranged and small because the positive charge of the muon is screened by the electron cloud in metals, a fact that is directly shown in Fig. 4 (see Appendix). Furthermore, Fig. 2 shows that the direct effect of relaxation on the value of B_c is tiny compared to the deviation between experiment and theory at this level of approximation. However, the reported results in this work are those of the relaxed lattice.

Finally, we want to determine the relative accuracy of the pseudo-wave-function (PS) spin densities compared to those obtained by the PAW reconstruction (PR) method described

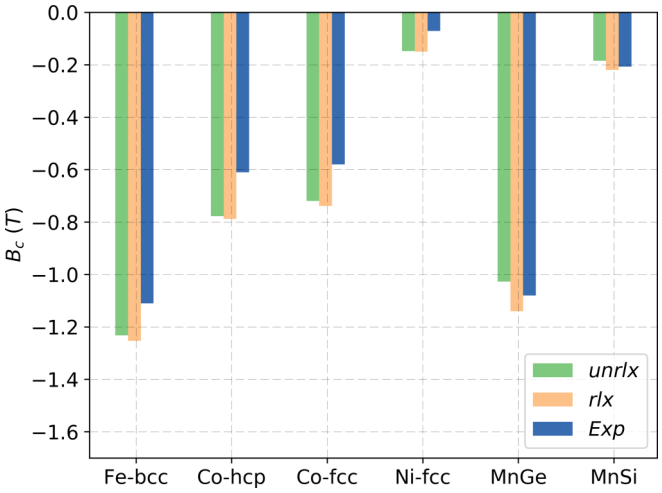

FIG. 2. Calculated muon contact hyperfine field B_c for unrelaxed ($unrlx$) and relaxed host atoms + muon at fixed cell volume (rlx) compared to the experimental value (Exp).

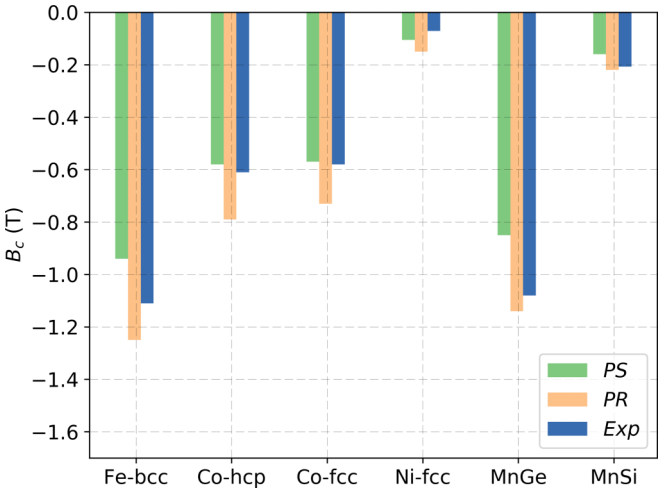

FIG. 3. Muon contact hyperfine field B_c calculated with the spin densities from the pseudo wave function (PS) and from the all-electron reconstruction with the PAW method (PR) compared to the experimental value (Exp).

in Sec. II. These are reported in the last two columns of Table I as $\rho_s^{PS}(\mathbf{r}_\mu)$ and $\rho_s^{PR}(\mathbf{r}_\mu)$, respectively, and the corresponding contact field is plotted in Fig. 3 and compared with the experimental values. The pseudo wave functions give results remarkably close to the experimental values, even though they do not include the actual core electron density. It should be noted, however, that this is probably due to an error compensation between the approximated core electronic density and the missing zero-point vibration corrections. In addition, the overshooting of all estimations obtained with PR is in agreement with the fact that corrections due to zero-point vibrations may lead to a reduction of the absolute value (as mentioned in Sec. II), thus systematically improving the agreement with the experimental data for all the compounds reported in Fig. 3.

A. Fe, Co, Ni

We have investigated the accuracy of the calculated magnetic moments and the effects of the muon on them. The experimental total magnetic moments of the transition 3d metals, shown in Table I, are well reproduced within the conventional GGA-DFT. The tabulated magnetic moments were estimated with the Löwdin population analysis [49]. With the muon impurity in the lattice, the moments of the nearest-neighbor host magnetic ions are negligibly perturbed. These perturbations contribute to no appreciable change of the calculated contact field. As we will further discuss, the contact field depends strongly on the accuracy of the calculated spin moments.

The first important result obtained is that the calculated spin imbalance at the muon, shown in Table I, is negative for all the considered metals, in agreement with experiment and with the simple notion that the majority spin electrons are in a direction opposite to the bulk magnetization at the muon. Furthermore, the deviations reported in Table II are on average 0.14 T and always within 0.2 T. This may be considered a rather good agreement, compared to results from the earlier works, since the averaging due to the muon's vibration is not included yet.

Admittedly, many of these earlier works [18,20,22,51] estimated the spin density at the muon site by a simple rescaling of the spin density of the bulk material at the position of the known muon site with an empirical spin enhancement factor that mimics the perturbation induced by the interstitial muon. This is clearly an unpractical ad hoc solution that impairs the *ab initio* method. They thus failed to establish the accuracy of the method over several materials.

TABLE I. Spin-only magnetic moment for each magnetic ion (without the muon) for the conventional GGA calculation m_{GGA}, the experimental value m_{exp}, and the reduced Stoner theory calculation (see Sec. III B) m_{RST} in units of μ_B; muon sites [24,34–38] in fractional coordinates; calculated spin density at the muon in atomic units of (a_0^{-3}) resulting from the pseudo wave function ρ_s^{PS} and the PAW reconstructed value ρ_s^{PR}.

Host metals [a]	m_{GGA}	m_{exp} [b]	m_{RST}	Muon site	$\rho_s^{PS}(\mathbf{r}_\mu)$	$\rho_s^{PR}(\mathbf{r}_\mu)$
Fe - bcc	2.17	2.22		0.50, 0.25, 0.00	−0.0179	−0.0238
Co - hcp	1.585	1.72		0.33, 0.67, 0.25	−0.0111	−0.0150
Co - fcc	1.645	1.59		0.50, 0.50, 0.50	−0.0109	−0.0139
Ni - fcc	0.638	0.606		0.50, 0.50, 0.50	−0.0020	−0.0028
MnGe	2.014	1.83	1.84	0.552, 0.552, 0.552	−0.0162	−0.0217
MnSi	1.00	0.4	0.401	0.541, 0.541, 0.541	−0.0031	−0.0042

[a]The MnGe and MnSi structure are of $P2_13$ space group (cubic) with the Mn atom at (0.138, 0.138, 0.138) crystal unit position.
[b]See Refs. [37–39].

TABLE II. Calculated static contact hyperfine field at the muon B_c by PAW reconstruction together with results from other works, experimental values B_c^{exp}, and deviations $\Delta^{exp} = B_c^{exp} - B_c$.

	B_c [T]			
Host metals	This work	Other works	exp	$\Delta^{exp}[T]$
Fe-bcc	−1.25	−0.94 [18]	−1.11 [34]	0.14
Fe-bcc		−1.01 [50]		
Fe-bcc		−1.44 [24]		
Fe-bcc		−1.03 [25]		
Co-hcp	−0.79	−1.34 [18]	−0.61 [35]	0.18
Co-hcp		−0.57 [50]		
Co-fcc	−0.73	−0.46 [24]	−0.58 [24]	0.15
Ni-fcc	−0.15	−0.69 [18]	−0.071 [36]	0.08
Ni-fcc		−0.059 [50]		
Ni-fcc		−0.13 [24]		
Ni-fcc		−0.31 [20]		
Ni-fcc		−0.059[21]		
MnGe	−1.14		−1.08 [37]	0.06
MnSi	−0.22		−0.207 [38]	0.013

In the earlier calculations, the large deviations between calculated and experimental contact field values (on average) were consistently attributed to the lack of muon zero-point motion correction. Our more accurate results indicate that the effect of the zero-point motion is needed but its extent is much smaller.

B. MnGe and MnSi

The muon implantation sites for MnSi and MnGe [37,38] are reported in Table I. Their zero-field magnetic structure, actually a spin spiral, was approximated by a collinear ferromagnetic state, since in both cases the pitch [37,38,52–54] is much longer than the lattice parameter.

The conventional DFT-calculated spin-only moment, m_{GGA}, deviates significantly from the experimental total magnetic moment for both B20 compounds and for MnSi in particular. This is a consequence of the poor standard DFT description of spin fluctuations in the magnetic ground state, especially for itinerant electron systems. This also affects the calculated spin density at the muon. For MnSi $m_{GGA} = 1.0\mu_B$, while the experimental value is $m_{exp} = 0.4\mu_B$. Notably, the ratio of these two values matches the ratio of the calculated and experimental contact fields for the calculated spin density of -0.0107 (a_0^{-3}). This is also the case for MnGe (see Table I), with calculated spin density -0.0251 (a_0^{-3}). Thus, the accuracy of the calculated contact field is heavily influenced by how well the host ground-state magnetization is reproduced by DFT. A simple but non–*ab initio* way to predict experimental contact field values would consist in rescaling the fields by the ratio m_{exp}/m_{GGA} or constraining the total moment of the bulk material [55] to the known experimental value.

Ab initio approaches have been discussed in the literature for MnSi. Attempts to obtain the experimental local moment by the reduction of the lattice constant within the local density approximation (LDA) [56] work only for unphysical lattice constant values. Hubbard U correction (DFT+U) to redistribute electrons between the majority and minority channels [57,58] acknowledge unphysical results in the pressure dependence of the magnetic moment (and we checked that the spin density at the muon departs from experiment).

A different approach was proposed by Ortenzi [59], who implemented a reduced Stoner theory (RST) modification to the exchange-correlation functionals. This approach involves the reduction of the *ab initio* Stoner parameter in the conventional spin-polarized DFT by a spin-scaling factor (ssxc) in the exchange-correlation potential. With this approach, the energy gain due to spin polarization within the conventional Stoner interaction criterion is reduced.

This method is variational and it adjusts the magnitude of the spin polarization for all standard functionals. We reimplemented it in the QUANTUM ESPRESSO code and obtained $m_{RST} \approx m_{exp}$ with ssxc values of 0.83 and 0.95, respectively, for MnSi and MnGe, as in Table I. The band structure remains negligibly changed, although bands are shifted in energy accordingly to the reduced Stoner parameter. Our results for the contact field, in good agreement with experiments, were obtained with spin densities calculated from this approach and are summarized in Table II.

IV. CONCLUSIONS

We have reviewed and validated a systematic approach to the calculation of the muon's static contact hyperfine field in metals to aid in μSR data analysis and understand the contact contribution to the hyperfine field of light impurities in metals.

We have successfully established the accuracy of the estimation of the muon contact field in metallic compounds with DFT. The pseudopotential DFT approach within the PAW formalism is good even for itinerant magnets, notoriously difficult systems.

The results may be affected by poor DFT reproduction of the magnetic moment which is common for these systems. The RST method allows a variational approach that may well reproduce the experimental results (both the magnetic moment and spin density) without forcing unphysical values of the other lattice quantities.

Our final results are obtained for an infinite muon mass and do not account for its finite zero-point vibrations. The full treatment of this aspect is beyond the scope of the present work, but we know that it has to reduce the absolute value of the static spin density. Therefore, the fact that the calculated value $|B_c^{exp}| - |B_c|$ is consistently small and negative agrees with the expected effect of zero-point vibrations. With this in mind the agreement between calculation and experiment is satisfactory at this level of approximation.

We conclude that DFT calculation of contact hyperfine fields is a viable assistance to μSR data analysis. Its standard implementation may well replace expensive, time-consuming, and often not readily available single-crystal measurements in the future.

ACKNOWLEDGMENTS

We thank Luciano Ortenzi for useful discussions. The calculations were performed with computing resources provided by STFC Scientific Computing Department's SCARF cluster, the

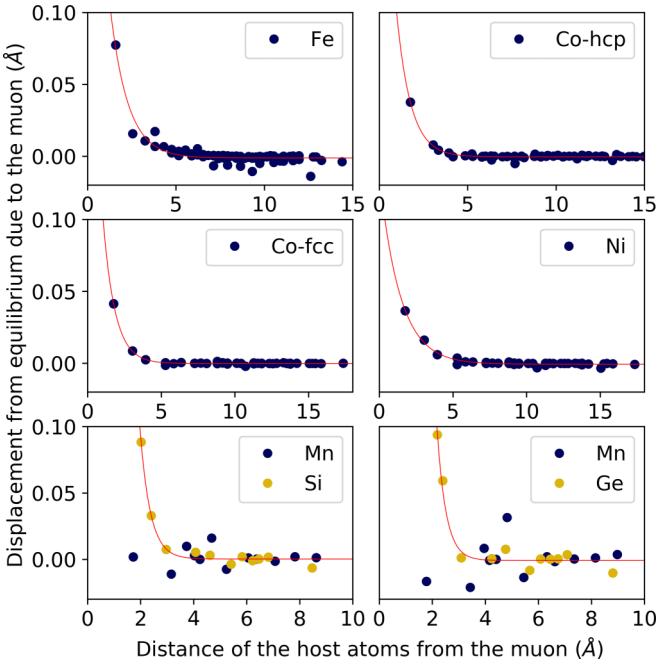

FIG. 4. Atomic displacement in the presence of the muon in a relaxed supercell vs the distance of each atom from the muon. Red lines are a guide to the eye showing the exponential decay.

Swiss National Supercomputing Centre (CSCS) under Project ID sm07, and the hpc resources at Università degli Studi di Parma, Italy. We also acknowledge grants from the H2020 Research Infrastructures under Grant Agreement No. 654000.

APPENDIX: SHORT-RANGE DISTORTION DUE TO THE MUON

The range of the lattice strain introduced by the interstitial muon defect may be directly quantified by comparing the position of each atom in the pristine material with their position in the supercell DFT calculation, after lattice relaxation with the muon. Figure 4 shows the difference of these two quantities versus the distance from the muon site. The top four panels display the result for the $4 \times 4 \times 4$ cell of the elemental metals, with a clear exponential decay on a length scale $\lambda < 1.25$ Å.

The data for the $2 \times 2 \times 2$ cell of the B20 compounds are more scattered, as expected in view of the presence of two different species. Interestingly, Si and Ge show a decaying displacement with $\lambda < 3.0$ Å, whereas Mn ions show no systematic deviation, perhaps indicating a much shorter value of λ.

[1] F.Bernardini, P. Bonfà, S. Massidda, and R. De Renzi, Phys. Rev. B **87**, 115148 (2013).
[2] J. S. Möller, D. Ceresoli, T. Lancaster, N. Marzari, and S. J. Blundell, Phys. Rev. B **87**, 121108 (2013).
[3] C. G. Van de Walle, Phys. Rev. Lett. **64**, 669 (1990).
[4] R. C. Vilão, A. G. Marinopoulos, R. B. L. Vieira, A. Weidinger, H. V. Alberto, J. P. Duarte, J. M. Gil, J. S. Lord, and S. F. J. Cox, Phys. Rev. B **84**, 045201 (2011).
[5] R. Khasanov, A. Amato, P. Bonfà, Z. Guguchia, H. Luetkens, E. Morenzoni, R. De Renzi, and N. D. Zhigadlo, Phys. Rev. B **93**, 180509 (2016).
[6] F. R. Foronda, F. Lang, J. S. Möller, T. Lancaster, A. T. Boothroyd, F. L. Pratt, S. R. Giblin, D. Prabhakaran, and S. J. Blundell, Phys. Rev. Lett. **114**, 017602 (2015).
[7] G. B. Pascua, Ph.D. thesis, Physik-Institut der Universität Zürich, 2014.
[8] P. Dalmas de Réotier, A. Maisuradze, A. Yaouanc, B. Roessli, A. Amato, D. Andreica, and G. Lapertot, Phys. Rev. B **93**, 144419 (2016).
[9] P. Dalmas de Réotier, A. Maisuradze, A. Yaouanc, B. Roessli, A. Amato, D. Andreica, and G. Lapertot, Phys. Rev. B **95**, 180403 (2017).
[10] A. Schenck and F. Gygax, in *Handbook of Magnetic Materials*, edited by K. H. J. Buschow (Elsevier Science B.V., Netherlands, 1995), Vol. 9, pp. 60–284.
[11] A. Yaouanc and P. Dalmas de Rotier, *Muon Spin Rotation Relaxation and Resonance: Applications to Condensed Matter* (Oxford University Press, Oxford, UK, 2011).
[12] J. S. Möller, P. Bonfà, D. Ceresoli, F. Bernardini, S. J. Blundell, T. Lancaster, R. De Renzi, N. Marzari, I. Watanabe, S. Sulaiman, and M. I. Mohamed-Ibrahim, Phys. Scr. **88**, 068510 (2013).
[13] P. Bonfà and R. De Renzi, J. Phys. Soc. Jpn. **85**, 091014 (2016).
[14] P. Bonfà, I. J. Onuorah, and R. D. Renzi, in *Proceedings of the 14th International Conference on Muon Spin Rotation, Relaxation and Resonance (muSR2017)*, JPS Conference Proceedings, Vol. 21 (The Physical Society of Japan, 2018), p. 011052.
[15] C. Slichter, *Principles of Magnetic Resonance*, Springer Series in Solid-State Sciences (Springer, Berlin, 1996), Chap. 4.
[16] F. Giustino, *Materials Modelling Using Density Functional Theory: Properties and Predictions* (Oxford University Press, Oxford, UK, 2014), Chap. 11.
[17] E. Daniel and J. Friedel, J. Phys. Chem. Solids **24**, 1601 (1963).
[18] P. Jena, Hyperfine Interact. **6**, 5 (1979).
[19] P. F. Meier, Helv. Phys. Acta **48**, 227 (1975).
[20] M. M. J. Rath, P. Jena, and C. Wang, Solid State Commun. **31**, 1003 (1979).
[21] B. D. Patterson and J. Keller, Hyperfine Interact. **6**, 73 (1979).
[22] P. Jena and M. Manninem, Hyperfine Interact. **9**, 405 (1981).
[23] S. Estreicher, A. Denison, and P. Meier, Hyperfine Interact. **8**, 601 (1981).
[24] B. Lindgren and D. E. Ellis, Phys. Rev. B **26**, 636 (1982).
[25] K. Terakura, H. Akaia, M. Akai, and J. Kanamori, The hyperfine field of the positive muons in the ferromagnetic transition metals, in *Electronic Structure and Properties of Hydrogen in Metals*, edited by C. B. Satterthwaite and P. Jena (Springer, New York, 1983), pp. 413–424.
[26] S. Blügel, H. Akai, R. Zeller, and P. H. Dederichs, Phys. Rev. B **35**, 3271 (1987).
[27] C. G. Van de Walle and P. Blóchl, Phys. Rev. B **47**, 4244 (1993).
[28] F. Mauri, B. G. Pfrommer, and S. G. Louie, Phys. Rev. Lett. **77**, 5300 (1996).
[29] C. J. Pickard and F. Mauri, Phys. Rev. B **63**, 245101 (2001).
[30] M. d'Avezac, N. Marzari, and F. Mauri, Phys. Rev. B **76**, 165122 (2007).

[31] R. Laskowski and P. Blaha, J. Phys. Chem. C **119**, 19390 (2015).
[32] M. Nusair, L. Wilk, and S. H. Vosko, J. Phys. F **11**, 1683 (1981).
[33] E. Pavarini and I. I. Mazin, Phys. Rev. B **64**, 140504 (2001).
[34] N. Nishida, R. S. Hayano, K. Nagamine, T. Yamazaki, J. H. Bewer, D. M. Garner, D. Fleming, T. Takeuchi, and Y. Ishikawa, Solid State Commun. **22**, 235 (1977).
[35] H. Graf, W. Kündig, B. D. Patterson, W. Reichart, P. Roggwiller, M. Camani, F. N. Gygax, W. Rüegg, A. Schenck, H. Schilling, and P. F. Meier, Phys. Rev. Lett. **37**, 1644 (1976).
[36] H. Graf, E. Holzschuh, E. Recknagel, A. Weidinger, and T. Wichert, Hyperfine Interact. **6**, 245 (1979).
[37] N. Martin, M. Deutsch, F. Bert, D. Andreica, A. Amato, P. Bonfà, R. De Renzi, U. K. Rößler, P. Bonville, L. N. Fomicheva, A. V. Tsvyashchenko, and I. Mirebeau, Phys. Rev. B **93**, 174405 (2016).
[38] A. Amato, P. Dalmas de Réotier, D. Andreica, A. Yaouanc, A. Suter, G. Lapertot, I. M. Pop, E. Morenzoni, P. Bonfà, F. Bernardini, and R. De Renzi, Phys. Rev. B **89**, 184425 (2014).
[39] C. Kittel, *Introduction to Solid State Physics*, 7th ed. (John Wiley and Sons, New York, 1996).
[40] P. Giannozzi, S. Baroni, N. Bonini, M. Calandra, R. Car, C. Cavazzoni, D. Ceresoli, G. L. Chiarotti, M. Cococcioni, I. Dabo, A. Dal Corso, S. de Gironcoli, S. Fabris, G. Fratesi, R. Gebauer, U. Gerstmann, C. Gougoussis, A. Kokalj, M. Lazzeri, L. Martin-Samos *et al.*, J. Phys.: Condens. Matter **21**, 395502 (2009).
[41] C. G. Van de Walle, P. J. H. Dentener, Y. Bar-Yam, and S. T. Pantelides, Phys. Rev. B **39**, 10791 (1989).
[42] P. E. Blöchl, Phys. Rev. B **50**, 17953 (1994).
[43] J. P. Perdew, K. Burke, and M. Ernzerhof, Phys. Rev. Lett. **77**, 3865 (1996).
[44] G. Breit, Phys. Rev. **35**, 1447 (1930).
[45] M. Battocletti, H. Ebert, and H. Akai, Phys. Rev. B **53**, 9776 (1996).
[46] N. Marzari, D. Vanderbilt, A. De Vita, and M. C. Payne, Phys. Rev. Lett. **82**, 3296 (1999).
[47] H. J. Monkhorst and J. D. Pack, Phys. Rev. B **13**, 5188 (1976).
[48] The quantum average of the spin density at the muon results in a *reduction* of the point value, since the spin density starts to decay away from that point.
[49] D. Sanchez-Portal, E. Artacho, and J. M. Soler, Solid State Commun. **95**, 685 (1995).
[50] J. Keller, Hyperfine Interact. **6**, 15 (1979).
[51] S. Estreicher and P. F. Meier, Phys. Rev. B **25**, 297 (1982).
[52] M. Deutsch, O. L. Makarova, T. C. Hansen, M. T. Fernandez-Diaz, V. A. Sidorov, A. V. Tsvyashchenko, L. N. Fomicheva, F. Porcher, S. Petit, K. Koepernik, U. K. Rößler, and I. Mirebeau, Phys. Rev. B **89**, 180407 (2014).
[53] Y. Ishikawa, K. Tajima, D. Bloch, and M. Roth, Solid State Commun. **19**, 525 (1976).
[54] O. L. Makarova, A. V. Tsvyashchenko, G. Andre, F. Porcher, L. N. Fomicheva, N. Rey, and I. Mirebeau, Phys. Rev. B **85**, 205205 (2012).
[55] T. Jeong and W. E. Pickett, Phys. Rev. B **70**, 075114 (2004).
[56] F. Carbone, M. Zangrando, A. Brinkman, A. Nicolaou, F. Bondino, E. Magnano, A. A. Nugroho, F. Parmigiani, T. Jarlborg, and D. van der Marel, Phys. Rev. B **73**, 085114 (2006).
[57] R. Collyer and D. Browne, Phys. B (Amsterdam, Neth.) **403**, 1420 (2008).
[58] K. V. Shanavas and S. Satpathy, Phys. Rev. B **93**, 195101 (2016).
[59] L. Ortenzi, I. I. Mazin, P. Blaha, and L. Boeri, Phys. Rev. B **86**, 064437 (2012).